Letter

Quasipolaron Surface Polarization in Bismuth Ferrite

Jiarui Zhang,[1] Yongbao Cui,[2] Nannan Liu,[3] Qi Qi,[1] Rui Huang,[1] Kai Chen,[1,4,*] Laijun Liu,[2,†] Zhida Han,[5,‡] and Guoliang Yuan[3]

[1] *School of Science, Nanjing University of Science and Technology, Nanjing 210094, People's Republic of China*
[2] *Guilin University of Technology, Guilin 541004, People's Republic of China*
[3] *School of Materials Science and Engineering, Nanjing University of Technology, Nanjing 210094, People's Republic of China*
[4] *MIIT Key Laboratory of Semiconductor Microstructure and Quantum Sensing, Nanjing University of Science and Technology, Nanjing 210094, People's Republic of China*
[5] *School of Electronic and Information Engineering, Changshu Institute of Technology, Changshu 215500, People's Republic of China*

(Received 29 July 2022; revised 21 September 2022; accepted 11 October 2022; published 8 November 2022)

With the introduction of a not fully screened polarization that leads to three magnetic subdomains nested in one ferroelectric domain, we identify it as the quasipolaron surface polarization in the electrode effect of bismuth ferrite. The remanent polarization at 40 Hz is about 439 μC/cm^2 in the dielectric hysteresis loop of a reverse S shape, accompanying the antiferromagnetic one of an S shape, which reveals that the surface is an indispensable part in spintronics.

DOI: 10.1103/PhysRevApplied.18.L051002

The room-temperature existence of long-range coupled ferroelectric and antiferromagnetic orders in multiferroic bismuth ferrite ($BiFeO_3$) manifests itself as a variety of attractive physical phenomena and technological potentials. Recently, within a single ferroelectric domain of about 6×6 μm in the last 30–50 nm of a (001)-oriented single crystal to its surface, triple-**k** magnetic subdomains of about 600×600 nm have been observed, which is due to a bulk **k** cycloid destabilized at the surface by a not fully screened polarization through magnetoelectric coupling [1]. The leakage polarization is unclear but important for the domain structure, when the nested domain structure offers a utilization for spintronics.

In $BiFeO_3$ with a slightly distorted rhombohedral structure (space group $R3c$), the Bi ions displace off-center about 0.61 Å for large dipoles of approximately 8.78 Debye units (D), pointing along one of the $\langle 111\rangle_r$ directions in the pseudocubic lattice. The broad distance distribution of 2.25–3.5 Å between Bi and neighbor O ions accommodates the disorder of local BiO_6 octahedra, with different octahedra rotation angles and Bi—O bond lengths [2]. The Bi sublattice is significantly more disordered than the Fe sublattice [3]. In FeO_6 octahedra with obvious short (1.92 Å) and long (2.15 Å) Fe—O bonding distances, the Fe ions shift off-center about 0.22 Å along the same directions for small dipoles of approximately 3.16 D. Oxygen ions are, in part, covalently bonded by O p states to both Bi and Fe ions [4–6], leading to $\langle 111\rangle_r$ oriented "--O–B_i–O–F_e–O--" dipole chains of alternating large and small dipoles, which are with a period of approximately $\sqrt{3} \times 6 \times 6$ μm. Along $\langle 111\rangle_r$ directions, the distance between the small dipole and the neighboring large one is in the range from approximately 3.08 to approximately 3.92 Å. Importantly, the disorder of local BiO_6 and FeO_6 octahedra provides crystalline positions of the energy double potential well for macroscopic polarization-switching dynamics. The existence of dipole chains is also suggested by the density-functional calculations of oxygen, bismuth, and iron vacancies [7]. The parallel branches of these dipole chains constitute the polarization, **P**, of ferroelectric domain along the $[111]_r$ axis, which makes the in-plane component on the $(111)_r$ surface plane. Although the strong coupling among the dipoles keeps the ferroelectric order against the thermal destruction up to the structural transition temperature of $T_c = 1033$ K, the multibody sensitivity of dipole chains to the ion number, the correlation strength, and the local crystal field result in different average values of spontaneous ferroelectric polarization,

*kai@njust.edu.cn
†ljliu@163.com
‡han @cslg.edu.cn

$\mathbf{P}_s$ (average dipole moment per unit volume), in the bulk, the film, the two-dimensional system, and the nanomaterial. The magnetic ground state is the antiferromagnetic cycloid, the plane of spin rotation in the cycloid is perpendicular to $\mathbf{P}_s$, and, thus, the $3d^5$ spins of Fe ions in dipole chains are perpendicular to the $\mathbf{P}_s$ branch of dipole chains. In the **k** direction also as the transverse direction of the branch, the superexchange interaction assists the strain and the relativistic Dzyaloshinskii-Moriya interaction, to correlate them up to the Neél temperature of $T_N = 643$ K. The dipole chains with different lengths have Fe $3d^5$ spins of different quantities, and to some extent have an effect on the average magnetic moment per unit cell. Thus, the three-dimensional dipole-chain network carrying the spins is formed as the bulk polarization at room temperature for the ferroelectricity [8–11]. The network is usually assumed as the result of boundary-optical phonon condensation, in which the short-range repulsion is compensated by the attractive long-range dipole-dipole interaction. The vibronic hybridization between Fe $3d$ and O $2p$ states drives the FeO_6 octahedra into Jahn-Teller distortion, and reduces such short-range repulsions with a narrower and better charge-transfer gap. The resultant p-d covalent energy gain makes charged ions off-center towards a long-range ferroelectric order. At present, there is no structural clue for the leakage polarization, which, firstly, is not fully screened by the bulk polarization and, secondly, involves magnetoelectric coupling. In this Letter, we identify the leakage polarization, and additionally reveal the quasipolaron and the reverse ferroelectricity, by comparing the effect of circular electrode materials and diameters on dielectric, polarization, and magnetic properties.

Samples of polycrystalline ceramics show the same basic characteristics as those of single crystals, but are more easily prepared, using the conventional solid-state reaction method. The starting metal oxides of Bi_2O_3 (99.99%) and Fe_2O_3 (99.9%) with stoichiometry, and an extra 2% Bi_2O_3 to compensate for the volatilization of Bi during the sintering stages, are mixed thoroughly in ethanol using ZrO_2 balls for 12 h, then dried and calcined at 650 °C for 6 h. The powders are ball-milled again for 12 h, mixed thoroughly with a polyvinyl alcohol (PVA) binder solution, and pressed into disks. All of them are sintered at 800 °C for 2 h in an atmosphere of O_2, and finally are observed to crystallize into the $R3c$ phase. Disk samples are polished to the same thickness of 0.5 mm. Ag and Au circular electrodes with diameters of 1.5, 3.0, and 6.0 mm are sputtered on one surface of disks as top electrodes. The same material as that of the top electrode is sputtered to fully cover the other face as the bottom electrode. Samples are denoted as Ag:1.5, Ag:3.0, Ag:6.0, Au:1.5, Au:3.0, and Au:6.0, respectively. Dielectric spectra are obtained using a Hewlett-Packard impedance/gain-phase analyzer (model 4294A, Agilent Co., USA). Dynamic hysteresis measurements are performed using a TF Analyzer 2000E and aixPlorer30_Software (aixACCT, Germany). Dc magnetization measurements are carried out using a commercial magnetic property measurement system (MPMS-3, Quantum Design, USA).

The material and diameter of circular electrodes have an obvious effect on the weak-field polarization, as a sign of which is the real part of the complex dielectric value, ε', i.e., the scientific form of industrial permittivity. For the Ag electrodes, a larger diameter reduces the value of ε', as shown in Fig. 1(a). The reduction is independent of frequency from 10^2 to 10^7 Hz, and the relative change defined as (ε'Ag/Au:1.5 or Ag/Au:3.0 − ε'Ag/Au:6.0)/ε'Ag:6.0 is as large as 83%, as shown in Fig. 1(b). However, the frequency-independent effect is not observed for the Au electrode samples, as shown in Figs. 1(c) and 1(d). For the Au:3.0 sample, an increased electrode diameter increases the value of ε' above the characteristic frequency of about 10^5 Hz, but decreases the value at lower frequencies. Also, the Au:6.0 sample shows a similar effect, the characteristic frequency being about 10^6 Hz.

To identify the weak-field polarization, complex plots of ε' and ε'' for all samples in a wide frequency range from 40 to 10^8 Hz are used, as shown in Fig. 2, where ε'' is the imaginary part of the complex dielectric value. There is a transition frequency (TF), at which two different decreasing and increasing trends of ε'' with increasing frequency are combined. For the Ag electrode samples

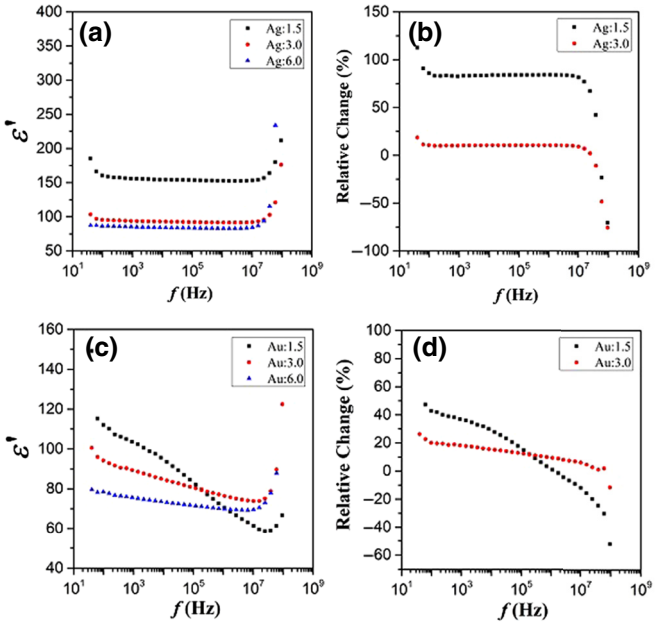

FIG. 1. Frequency dependence of ε' and relative change, for all samples in a wide frequency range from 40 Hz to 10^8 Hz at room temperature.

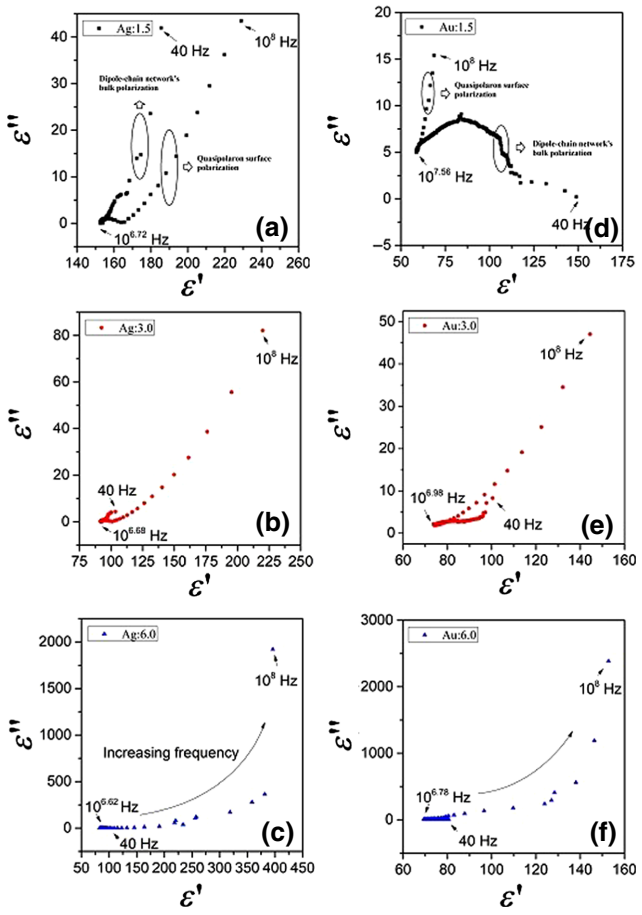

FIG. 2. Complex plots of ε' and ε'' for all samples.

[Figs. 2(a)–2(c)], the TF is $10^{6.72}$ Hz for the Ag:1.5 sample, $10^{6.68}$ Hz for the Ag:3.0 one, and $10^{6.62}$ Hz for the Ag:6.0 one, respectively. Thus, increasing electrode diameter decreases the TF, and then increases the higher-frequency response range of the polarization. The same phenomenon occurs for all of the Au electrode samples [Figs. 2(d)–2(f)]. For magnetoimpedance spectroscopy on the films, the equivalent circuit-fitting method, in a phenomenological way, shows two types of polarizations, which are due to the intrinsic contribution and the extrinsic interface one [12]. Within the frame of the classic dielectric theory [13], the intrinsic contribution is the dipole-chain network, and the extrinsic one is the interface Schottky-type barrier, which is, however, ambiguous for dielectric species. Quantum dielectric physics, further, gives a clearer hint that the barrier results from the electrostatic potential field of polaronlike $3d$ electrons pinned at grain surfaces [14]. The local polarization of these electrons is proposed by the superexchange theory [15], and in bismuth ferrite is particularly highlighted by the non-d^0 ferroelectric polarization of the semicovalent superexchange model [16]. The maximum strength of the superexchange interaction in the half-filling $t_{2g}^3 e_g^2$ configuration of Fe $3d^5$ electrons and the strong interatomic hybridization by Fe 3d and O $2p$ orbital overlap enhance the Born effective charge, with decreasing the moment on Fe ions through the covalent exchange pairing and corroborating the antiferromagnetic pairing's facilitation to the formation of singlet states, and thus resulting in the long-range ferroelectric order in Fe $3d^5$ multiorbital manifold. The superexchange endows $BiFeO_3$ with a $3d^5$-electron-driven ferroelectric polarization, which is as large as approximately 53 $\mu C/cm^2$ for the total polarization (approximately 100 $\mu C/cm^2$) when the polarization induced by the dipole chains is estimated as approximately 47 $\mu C/cm^2$. The hopping routes for the superexchange include ligand holes, and terminate at the orbitals in the surface unit cells. We name these $3d$ electrons as quasipolarons, and thus the quasipolaron surface polarization may be a candidate for the leakage polarization. Increased electrode diameter means that more quasipolarons are involved in the dielectric polarization at high frequencies, which requires more excitation energy, and then the decreased TF is understandable for the wider high-frequency response range. Notably, the quasipolarons of the surface polarization originate from the Fe $3d^5$ electrons of dipole chains, and macroscopically the TF confirms that the quasipolaron surface polarization is correlated to the bulk one of the dipole-chain network.

The quasipolaron surface polarization at higher frequencies is affected by the electrode characteristics, and via correlation, may transfer the effect to the bulk polarization of the dipole-chain network under lower-frequency strong fields. To validate this, we present the frequency-dependent dielectric hysteresis loops, i.e., the polarization-voltage loops, when an excitation signal of periodic and triangular wave with the same amplitude of 3600 V is applied, and all of the current range is set as 100 mA. The chosen frequency range from 40 to $10^{3.6}$ Hz encompasses the response of the bulk polarization, as suggested by weak-field dielectric spectra. Figures 3(a) and 3(d)–3(f) show that the almost frequency-independent loops are in the shape of a "banana" for samples Ag:1.5, Au:1.5, Au:3.0, and Au:6.0, with a polarization as large as approximately 4 $\mu C/cm^2$. The shape suggests that the loops are dominated by leakage currents, which results from the mixed valence of Fe^{2+} and Fe^{3+} within the frame of the semicovalent superexchange model. The measured current is more underflow than 100 mA, and the samples are lossy dielectrics [17]. When the dielectrics are measured as the internal layer of a parallel-plate capacitor with two metal electrodes, we summarize the switched charge Q, the measured current I, and P in one period, T (1/frequency), as the following:

$$Q = (\int IdT)\,A = \left(\int I_{\text{bulk}}dT + \int I_{\text{leakage}}dT\right)A = (P_{\text{bulk}} + P_{\text{surface}})A, \quad (1)$$

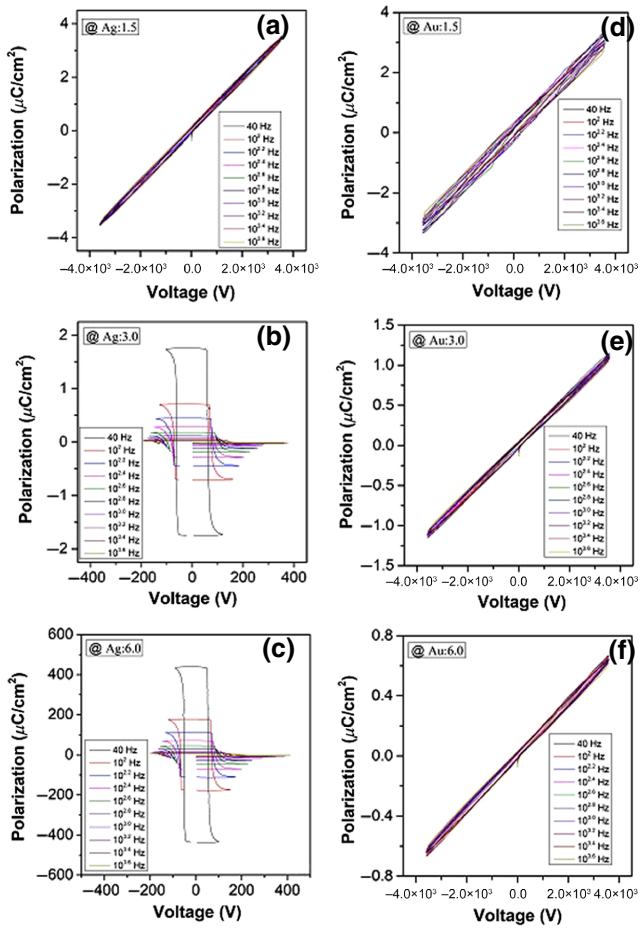

FIG. 3. Polarization-voltage loops under the same voltage of 3600 V at different frequencies for all samples.

where P_{bulk} is the bulk polarization, P_{surface} is the surface polarization, and A is the lateral area of the capacitor. We assume that all basic properties follow the linear superposition rule and choose the plus sign to describe the relation of the same kind. Further, the plus sign shows the correlation between the remanent bulk polarization of dipole-chain network and the remanent surface polarization of quasipolarons. By correlation, an increased electrode diameter decreases both the value and the range of **P** from that of sample Au:1.5, then to that of sample Au:3.0, and finally to that of sample Au:6.0, as shown in Figs. 3(d)–3(f). The trend seems to be that the value range is inversely proportional to the electrode diameter. A similar trend also occurs for sample Ag:1.5 and sample Ag:3.0 [Figs. 3(a) and 3(b)]; however, the shape of the dielectric hysteresis loop changes from a "banana" shape for sample Ag:1.5 to a reverse S shape for sample Ag:3.0. Sample Ag:6.0 also shows dielectric hysteresis loops of the reverse S shape, as shown in Fig. 3(c). Although the measured current is underflow in sample Ag:3.0, that in sample Ag:6.0 is neither underflow nor overflow, and therefore the measured polarization-voltage loop is reliable. We notice that the recorded largest voltage of approximately 400 V is much smaller than the applied amplitude of 3600 V, and this screening effect confirms the existence of quasipolaron surface polarization.

Interesting, the remanent polarization, $\mathbf{P}_r$, at 40 Hz is about 439 μC/cm^2, which is the largest value. The characteristic remanent polarization, $\mathbf{P}_{\text{cr}}$, is defined as follows:

$$P_{\text{cr}} = |P_{r+} - P_{r-}|/2, \tag{2}$$

where P_{r+} and P_{r-} are the positive and negative remanent polarizations, respectively.

Then, it is dependent on the excited frequency [Figs. 4(a) and 4(b)], as follows:

$$\lg(P_{\text{cr}}) = -\lg(f) + 1.87 \text{ for sample Ag:3.0}, \tag{3}$$

$$P'_{\text{cr}} = P'_0(E'_0/hf) = P'_0(E'_0/\hbar\omega) \tag{4}$$

$$(P'_0 = 10^{1.87}\tau'_0, E'_0 = h/\tau'_0, \text{ and } \omega = 2\pi f),$$

$$\lg(P_{\text{cr}}) = -\lg(f) + 4.26 \text{ for sample Ag:6.0}, \tag{5}$$

$$P''_{\text{cr}} = P''_0(E''_0/hf) = P''_0(E''_0/\hbar\omega) \tag{6}$$

$$(P''_0 = 10^{4.26}\tau''_0, E''_0 = h/\tau''_0, \text{ and } \omega = 2\pi f),$$

where P'_0 is the polarization of surface ground-state quasipolarons, E'_0 is the ground-state energy, h is the Planck constant, f is the applied voltage frequency, $\hbar$ is the reduced Planck constant, ω is the angular frequency, and τ'_0 is the retention time of the ground-state quasipolarons in sample Ag:3.0. The same applies to P''_0, E''_0, and τ''_0 for sample Ag:6.0.

Finally, they are summarized as follows:

$$P^l_{cr} = P^l_0(E^l_0/hf) = P^l_0(E^l_0/\hbar\omega) \tag{7}$$

$(l = 1.87$ for sample Ag:3.0 and 4.26 for sample Ag:6.0).

By increasing the excitation frequency, the entities of dipole chains are excited from the ground state to fewer states of higher energy level, which reduces the quasipolaron occupy quantity to $\mathbf{P}_{\text{cr}}$, accompanying a screening effect whereby the polarization contribution at lower-energy-level states is shielded. The higher the energy level, the fewer the states and they are quasicontinuous or continuous. Thus, we induce the dielectric hysteresis loop of the reverse S shape as the reverse ferroelectricity, which is dominated by the quantum excited states. To further distinguish the reverse ferroelectricity from ferroelectricity, we plot the time dependence of measured

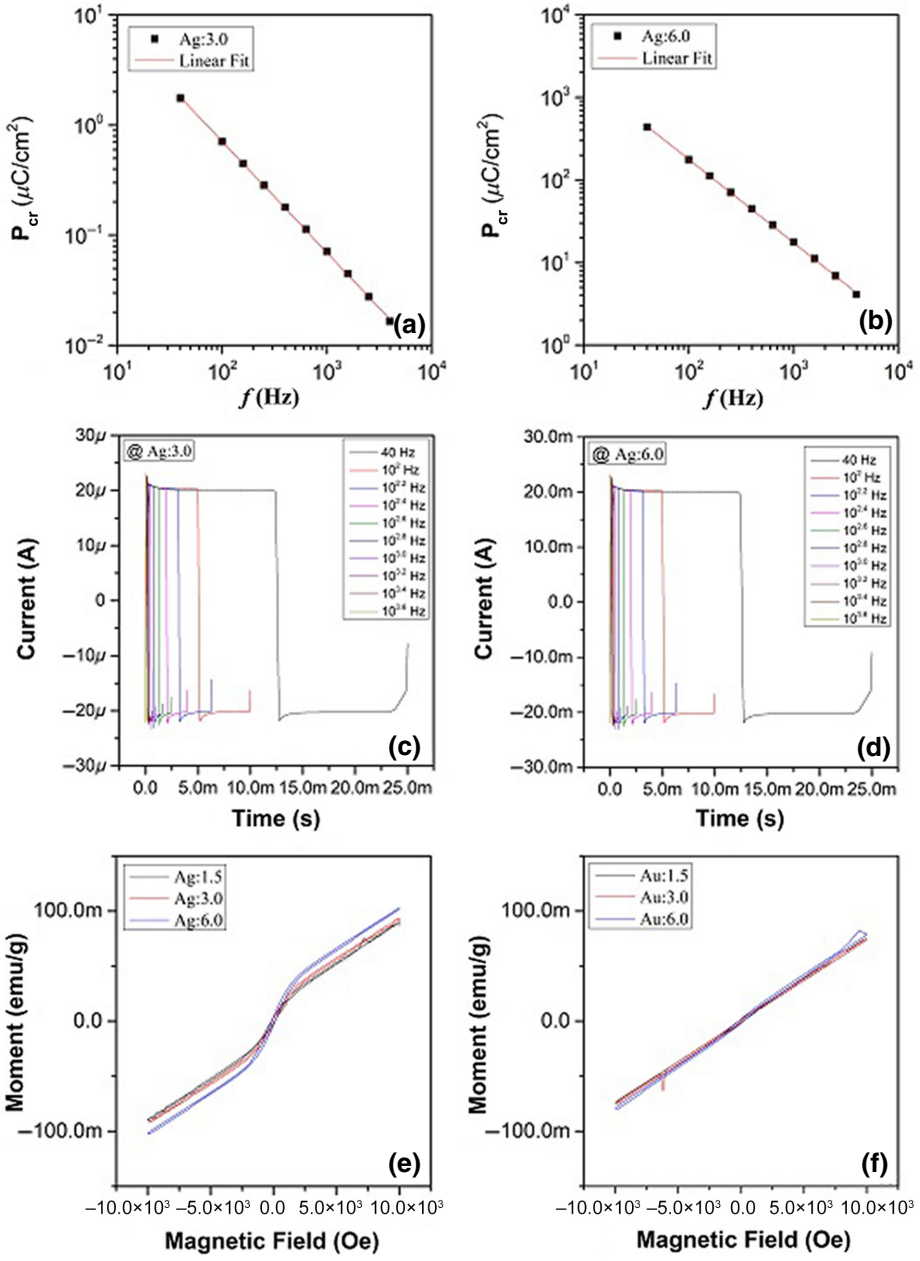

FIG. 4. Frequency dependence of $\mathbf{P}_{cr}$ and time dependence of measured current in one period for the sample Ag:3.0 (a and c) and the sample Ag:6.0 (b and d), respectively. Magnetic hysteresis loops for all samples (e and f).

current in one period, according to Eq. (1). As shown in Figs. 4(a) and 4(b), the dependence shows a doorframe shape, which is different from the M shape of ferroelectricity. The large current in Fig. 4(b) shows that compared with those in other samples, more quasipolarons in sample Ag:6.0 are excited to involve the surface polarization. And these quasipolarons are with spins, and thus sample Ag:6.0 should show a better magnetic property, which is self-consistently confirmed by the magnetic hysteresis loop of S shape, as shown in Figs. 4(e) and 4(f). Under the same magnetic field of 10 kOe, these quasipolarons improve the moment of sample Ag:6.0 by up to 37% compared with those of other samples.

In summary, the quasipolaron surface polarization is revealed as the origin for the nested domain structure, when the electrode effect is compared, and the concepts of quasipolaron and reverse ferroelectricity are introduced. More quasipolarons are pinned at the surface per unit area, increasing the surface density of antiferromagnetically ordered spins. The largest remanent polarization and the better antiferromagnetic properties show that the surface is important for spintronics.

Acknowledgments.—J.Z. and Y.C. contributed equally to the work. K.C. acknowledges the support from the National Natural Science Foundation of China (Grant No. 11004106) and the Fundamental Research Funds for the Central Universities (Grant No. 30920021144).

[1] Aurore Finco, Angela Haykal, Stéphane Fusil, Pawan Kumar, Pauline Dufour, Anne Forget, Dorothée Colson, Jean-Yves Chauleau, Michel Viret, Nicolas Jaouen, Vincent Garcia, and Vincent Jacques, Imaging Topological Defects in a Noncollinear Antiferromagnet, Phys. Rev. Lett. **128**, 187201 (2022).

[2] A. Palewicz, P. Rrzenioslo, I. Sosonowska, and A. W. Hewat, Atomic displacements in $BiFeO_3$ as a function of temperature: Neutron diffraction study, Acta Crystallogr. Sect. B **63**, 537 (2007).

[3] S. Chattopadhyay, S. D. Kelly, V. R. Palkar, L. Fan, and C. U. Segre, Investigation of size effects in magnetoelectric $BiFeO_3$, Phys. Scr. **T115**, 709 (2005).

[4] R. Saeterli, S. M. Selbah, P. Ravindran, T. Grande, and R. Holmestad, Electronic structure of multiferroic $BiFeO_3$ and related compounds: Electron energy loss spectroscopy and density functional study, Phys. Rev. B **82**, 064102 (2010).

[5] D. Ricinschi, K.-Y. Yun, and M. Okuyama, A mechanism for the 150 $\mu C/cm^{-2}$ polarization of $BiFeO_3$ films based on first-principles calculations and new structural data, J. Phys.: Condens. Matter **18**, L97 (2006).

[6] I.-T. Bae, A. Kovacs, H. J. Zhao, J. Iniguez, Sh. Yasui, T. Ichinose, and H. Naganuma, Elucidation of crystal and electronic structures within highly strained $BiFeO_3$ by transmission electron microscopy and first-principles simulation, Sci. Rep. **7**, 46498 (2017).

[7] Grégory Geneste, Charles Paillard, and Brahim Dkhil, Polarons, vacancies, vacancy associations, and defect states in multiferroic $BiFeO_3$, Phys. Rev. B **99**, 024104 (2019).

[8] J. T. Han, Y.-H. Huang, X.-J. Wu, C.-L. Wu, W. Wei, B. Peng, W. Huang, and J. B. Goodenough, Tunable synthesis of bismuth ferrites with various morphologies, Adv. Mater. **18**, 2145 (2006).

[9] S. V. Kiselev, R. P. Ozerov, and G. S. Zhdanov, Detection of magnetic order in ferroelectric $BiFeO_3$ by neutron diffraction, Sov. Phys. Dokl. **7**, 742 (1963).

[10] I. H. Lone, J. Aslam, N. R. E. Radwan, A. H. Bashal, A. F. Ajlou, and A. Ajhter, Multiferroic ABO3 transition metal oxides: A rare interaction of ferroelectricity and magnetism, Nano Res. Lett. **14**, 142 (2019).

[11] Y. Yin and Q. Li, A review on all-perovskite multiferroic tunnel junctions, J. Materiomics **3**, 245 (2017).

[12] R. Schmidt, J. Ventura, E. Langenberg, N. M. Nemes, C. Munuera, M. Varela, M. Garcia-Hernandez, C. Leon, and J. Santamaria, Magnetoimpedance spectroscopy of epitaxial multiferroic thin films, Phys. Rev. B **86**, 035113 (2012).

[13] A. K. Jonscher, *Dielectric Relaxation in Solids* (Chelsea Dielectrics, London, 1983).

[14] J.-R. Zhang, Y.-Q. Li, Q.-R. Yang, Y.-W. Yang, F.-Q. Meng, T.-F. Wang, Z. Xia, Y. Wang, K. Chen, Q.-H. Zhang, *et al.*, A structural perspective on giant permittivity $CaCu_3Ti_4O_{12}$: One way to quantum dielectric physics in solids, Open Ceram. **6**, 100126 (2021).

[15] P. W. Anderson, New approach to the theory of superexchange interactions, Phys. Rev. **115**, 2 (1959).

[16] Y. Shen, X.-G. Wan, Q.-B. Zhao, G. Li, and C.-G. Duan, Non-d^0 ferroelectricity from semicovalent superexchange in bismuth ferrite, Phys. Rev. B **104**, 024421 (2021).

[17] J. F. Scott, Ferroelectrics go bananas, J. Phys.: Condens. Matter **20**, 021001 (2008).